# Topology of magnetars external field – I. Axially symmetric fields

L. Pavan,[1]⋆ R. Turolla,[1,2,3] S. Zane[2] and L. Nobili[1]

[1]*Department of Physics, University of Padova, via Marzolo 8, 35131 Padova, Italy*
[2]*Mullard Space Science Laboratory, University College London, Holmbury St. Mary, Dorking, Surrey, RH5 6NT, UK*
[3]*INFN, Sezione di Padova, via Marzolo 8, 35131 Padova, Italy*

**ABSTRACT**

There is an increasing theoretical and observational evidence that the external magnetic field of magnetars may contain a toroidal component, likely of the same order of the poloidal one. Such 'twisted magnetospheres' are threaded by currents flowing along the closed field lines which can efficiently interact with soft thermal photons via resonant cyclotron scatterings (RCS). Actually, RCS spectral models proved quite successful in explaining the persistent $\sim$1–10 keV emission from the magnetar candidates, the soft $\gamma$-ray repeaters (SGRs) and the anomalous X-ray pulsars (AXPs). Moreover, it has been proposed that, in the presence of highly relativistic electrons, the same process can give rise to the observed hard X-ray spectral tails extending up to $\sim$200 keV. Spectral calculations have been restricted up to now to the case of a globally twisted dipolar magnetosphere, although there are indications that the twist may be confined only to a portion of the magnetosphere, and/or that the large-scale field is more complex than a simple dipole. In this paper, we investigate multipolar, force–free magnetospheres of ultramagnetized neutron stars. We first discuss a general method to generate multipolar solutions of the Grad-Schlüter-Shafranov (GSS) equation, and analyse in detail dipolar, quadrupolar and octupolar fields. The spectra and lightcurves for these multipolar, globally twisted fields are then computed using a Monte Carlo code and compared with those of a purely dipolar configuration. Finally, the phase-resolved spectra and energy-dependent lightcurves obtained with a simple model of a locally sheared field are confronted with the *International Gamma-Ray Astrophysics Laboratory* (*INTEGRAL*) observations of the AXPs 1RXS J1708−4009 and 4U 0142+61. Results support a picture in which the field in these two sources is not globally twisted.

**Key words:** stars: magnetic fields – stars: neutron – X-rays: stars.

## 1 INTRODUCTION

Among isolated neutron stars (INSs), a small number of objects, namely the soft $\gamma$-ray repeaters (SGRs) and the anomalous X-ray pulsars (AXPs), share a number of common, peculiar characteristics. These are the huge spin down rates, $\dot{P} \sim 10^{-10}$–$10^{-13}$ s s$^{-1}$, absence of radio emission (till now only the AXPs XTE J1810−197 and 1E 1547.0−5408 have been detected in the radio, Camilo et al. 2007a,b), persistent X-ray luminosities in the range $L \sim 10^{34}$–$10^{36}$ erg s$^{-1}$ and rotational periods $P \sim 2$–12 s, a very narrow range compared with that of other classes of INSs. Though SGRs activity is higher, both groups undergo erratic X/$\gamma$-ray bursts with peak luminosities of $\sim$10$^{40}$–10$^{41}$ erg s$^{-1}$ and typical durations of $\sim$ 0.1–1 s. Moreover, SGRs exhibit much more energetic events, the so-called giant flares (GFs), in which energies up to $\sim$10$^{47}$ erg are released in

a time-scale of 1 s (see, for a recent review, Mereghetti 2008). Thanks to *International Gamma-Ray Astrophysics Laboratory* (*INTEGRAL*) and *Rossi X-Ray Timing Explorer* (*RXTE*), AXPs and SGRs are now known to be also persistent hard X-ray sources (e.g. Kuiper, Hermsen & Mendez 2004; Mereghetti et al. 2005; Götz et al. 2006; Kuiper et al. 2006). Actually, their energy output in the $\sim$20–200 keV range may amount to as much as 50 per cent of the total flux emitted above $\sim$1 keV. Recent, deeper *INTEGRAL* observations have shown that the hard X-ray emission is highly phase-dependent and probably results from the superposition of different spectral components (Den Hartog et al. 2008a; Den Hartog, Kuiper & Hermsen 2008b).

At variance with radio-pulsars, the persistent emission of SGRs/AXPs is $\sim$10–100 times higher than their rotational energy losses. This, together with the lack of detected stellar companions, indicates that the persistent emission of these sources is unlikely to be powered by rotation or accretion. The (dipolar) magnetic fields inferred from the spin-down measurements, $B \sim 10^{14} - 10^{15}$ G,

⋆E-mail: lucia.pavan@unipd.it

largely in excess of the quantum critical field ($B_Q = 4.4 \times 10^{13}$ G), support the idea that SGRs and AXPs are ultramagnetized NSs (or magnetars; Duncan & Thompson 1992; Thompson & Duncan 1993) and their (persistent and bursting) emission is sustained by the super-strong magnetic field. Although other scenarios, mainly based on accretion from a debris disc left after the supernova event (e.g. Alpar 2001; Ekşi & Alpar 2003; Ertan & Alpar 2003), may still be considered, the magnetar model appears capable of explaining in a simple and economical way most of the observed properties of SGRs and AXPs (e.g. Woods & Thompson 2006).

In a magnetar with surface field $\sim 10^{15}$ G, the internal field can reach $\sim 10^{17}$ G (Thompson & Duncan 1993, 1995). Since the poloidal and toroidal components are expected to be in rough equipartition [see Thompson et al. 2002 (hereafter TLK), and references therein], the huge toroidal field stresses the crust, producing a deformation of the surface layers. This, in turn, induces a rotation of the external field lines which are anchored to the star crust and leads to the appearance of an external toroidal component. The properties of such a twisted magnetosphere have been investigated by TLK by means of a model analogous to that for the solar magnetic field (e.g. Low & Lou 1990; Wolfson 1995, hereafter W95) under the assumptions of a static, dipolar, globally twisted field and enforcing, as in the solar models, the force–free condition.

A feature of (non-potential) force–free fields is the presence of supporting currents. As first suggested by TLK, thermal photons emitted by the star surface can scatter at the cyclotron resonance on the charges flowing in the magnetosphere, and this can drastically alter the primary spectrum. Recent, detailed calculations [Lyutikov & Gavriil 2006; Fernandez & Thompson 2007; Nobili et al. 2008a (NTZ hereafter)] of scattering onto mildly relativistic electrons confirmed this picture. Typical synthetic spectra exhibit a high-energy tail, superimposed to a thermal bump and closely resemble the (empirical) 'blackbody+power-law' model which has been routinely used to describe the magnetars quiescent emission in the $\sim$0.5–10 keV band (see again Woods & Thompson 2006 and Mereghetti 2008 for a summary of observational results). This model has been successfully applied to the X-ray spectra of several AXPs/SGRs by Rea et al. (2008, see also NTZ), providing direct support to the twisted magnetosphere scenario.

The origin of the high-energy tails discovered with *INTEGRAL* is much less understood. Thompson & Beloborodov (2005) analysed different mechanisms within the magnetar model, and suggested that the hard X-rays may be produced either by thermal bremsstrahlung in the surface layers heated by returning currents or by synchrotron emission from pairs created higher up in the magnetosphere. Quite interestingly, Baring & Harding (2007, 2008) have recently proposed a further possibility, according to which the soft gamma-rays may also originate from resonant upscattering of seed photons, if a population of highly relativistic electrons is present in the magnetosphere (see also Nobili, Turolla & Zane 2008b).

Since the conduction current in a sheared magnetosphere is $\propto \nabla \times \boldsymbol{B}$, the particle density and hence the optical depth to resonant scattering depends on the shear TLK. Moreover, the global topology of the magnetic field influences scattering even for fixed shear. A globally twisted dipolar field will in general give rise to a different spectrum from that of a globally twisted quadrupolar field with the same twist angle. Because the spatial distribution of charges is not homogeneous (TLK), changes in shear and/or field topology are going to produce differences not only in the spectral shape, but also in the pulse shape of the received radiation. Some complicated pulse profiles from SGRs have already been explained by invoking higher order multipoles (e.g. Feroci et al. 2001; Thompson &

Duncan 2001). Moreover, recent data, both for AXPs and SGRs, seem to point towards the presence of a localized, rather than global, twist (e.g. Woods et al. 2007; Perna & Gotthelf 2008). However, no investigation, which includes multipolar components or localized twists, has been presented till now.

In this paper, we discuss how globally twisted magnetostatic equilibria can be derived in the case of higher order, axially symmetric multipolar fields. In particular, explicit (numerical) solutions for quadrupolar and octupolar fields are presented. We use the Monte Carlo code developed by NTZ to investigate the properties of the emerging spectrum and pulse profiles for higher order multipolar fields. The paper is organized as follows. In Section 2, we introduce the globally twisted model and derive the solutions for each axially symmetric multipole; an analytical solution, valid in the case of dipolar and quadrupolar fields for small shear, is presented in Appendix A. Monte Carlo spectra and lightcurves obtained with different force–free magnetospheric configurations are discussed in Section 3, where a comparison with the timing properties of the hard X-ray emission from the AXPs 1RXS J1708−4009 and 4U 0142+6 is also presented. Discussion follows in Section 4.

## 2 GLOBALLY-TWISTED AXISYMMETRIC MODELS

In this section, we present the basic equations that we use to derive globally-twisted magnetospheric models. We closely follow the approach outlined in W95 and TLK, who considered the global twist of a dipolar field. As we show below, the same approach can be used to compute twisted fields for multipoles of arbitrary order. As in W95 and TLK, we restrict to magnetostatic, force–free equilibria. In the case of a low density, static plasma, in fact, in the standard magnetohydrodynamics equation

$$\rho \frac{\partial \boldsymbol{v}}{\partial t} + \rho(\boldsymbol{v} \cdot \nabla)\boldsymbol{v} = -\nabla p + \rho \boldsymbol{g} + \boldsymbol{j} \times \boldsymbol{B},$$

where $\rho$ and $\boldsymbol{v}$ are the plasma density and velocity, the velocity and gravity terms can be neglected. With the further hypothesis that the (plasma) pressure force is small with respect to the Lorentz force $\boldsymbol{j} \times \boldsymbol{B}$ (where $\boldsymbol{j}$ is the current density), the equation reduces to $\boldsymbol{j} \times \boldsymbol{B} = 0$. Since we are interested in stationary configurations, the Ampére–Maxwell equation simplifies to $\nabla \times \boldsymbol{B} = (4\pi/c)\,\boldsymbol{j}$. From the two previous conditions, the usual expression for the force–free condition is recovered:

$$(\nabla \times \boldsymbol{B}) \times \boldsymbol{B} = 0. \tag{1}$$

Our aim is to construct an axisymmetric, force–free field by adding a defined amount of shear to a potential field. In accordance with both TLK and W95, we choose to use the flux function $\mathscr{P}$ to express the poloidal component of the field. Axisymmetry is enforced choosing a function independent of the azimuth $\phi$ (we use a spherical coordinate system with the polar axis along the magnetic moment vector). Thus, the general expression for an axisymmetric field is

$$\boldsymbol{B} = \frac{\nabla \mathscr{P}(r, \theta) \times \hat{\boldsymbol{e}}_\phi}{r \sin \theta} + B_\phi(r, \theta)\hat{\boldsymbol{e}}_\phi, \tag{2}$$

where $\hat{\boldsymbol{e}}_\phi$ is the unit vector in the $\phi$ direction.

By inserting the previous expression into the force–free condition (equation 1), one obtains two independent scalar equations for the flux function, $\mathscr{P}$, and the toroidal component of the field, $B_\phi$. The former requires $B_\phi$ to be a function of $\mathscr{P}$ only (Low & Lou 1990),

thus we can write

$$B_\phi(r, \theta) = \frac{1}{r \sin \theta} F(\mathscr{P}), \tag{3}$$

where $F$ is an arbitrary function. Introducing the previous expression into the second scalar equation leads to the Grad-Schlüter-Shafranov (GSS) equation

$$\frac{\partial^2 \mathscr{P}}{\partial r^2} + \frac{1 - \mu^2}{r^2} \frac{\partial^2 \mathscr{P}}{\partial \mu^2} + F(\mathscr{P}) \frac{\mathrm{d}F}{\mathrm{d}\mathscr{P}} = 0 \tag{4}$$

(here and in the following $\mu \equiv \cos\theta$).

The GSS equation can be reduced to an ordinary differential equation (ODE) by making suitable assumptions on the dependence of $\mathscr{P}$ on the coordinates. Following a classical approach to this problem (e.g. Low & Lou 1990, W95, TLK), we assume separation of variables and choose the flux function $\mathscr{P}$ in the form

$$\mathscr{P} = \mathscr{P}_0 \left( \frac{r}{R_{\mathrm{NS}}} \right)^{-p} f(\mu), \tag{5}$$

where $f(\mu)$ is a function of the colatitude $\theta$, $R_{\mathrm{NS}}$ is the stellar radius and $\mathscr{P}_0 = B_{\mathrm{pole}} R_{\mathrm{NS}}^2 / 2$, as in TLK. The requirement that all the components of $\boldsymbol{B}$ have the same radial dependence implies that

$$F(\mathscr{P}) = \sqrt{\frac{C}{p(1 + p)}} \mathscr{P}^{1 + 1/p}, \tag{6}$$

where, for later convenience, we have expressed the multiplicative constant in terms of a parameter $C$ and of the radial exponent $p$. Recalling equation (2), one can explicitly write the magnetic field as a function of $f$:

$$\boldsymbol{B} = \frac{B_{\mathrm{pole}}}{2} \left( \frac{r}{R_{\mathrm{NS}}} \right)^{-p-2} \left[ -f', \frac{pf}{\sin\theta}, \sqrt{\frac{Cp}{p+1}} \frac{f^{1+1/p}}{\sin\theta} \right], \tag{7}$$

where a prime denotes derivation with respect to $\mu$. Finally, taking into account equations (5) and (6), the GSS equation becomes for the case at hand

$$(1 - \mu^2) f'' + p(p + 1) f + C f^{1+2/p} = 0, \tag{8}$$

which is a second order ordinary differential equation for the angular part of the flux function. Its solution, once a suitable set of boundary conditions has been supplied (see Section 2.1), completely specifies the external magnetic field.

Besides controlling the radial decay, the parameter $p$ also fixes the amount of shear of the field. In fact, recalling the definition of shear angle (W95, TLK),

$$\Delta\phi_{\mathrm{NS}} = \int_{\mathrm{fieldline}} \frac{B_\phi}{(1 - \mu^2) B_\theta} \mathrm{d}\mu$$

$$= \left[ \frac{C}{p(1 + p)} \right]^{1/2} \int_{\mathrm{fieldline}} \frac{f^{1/p}}{1 - \mu^2} \mathrm{d}\mu, \tag{9}$$

it is immediate to see that different values of $p$ correspond to fields with different shear. Actually, as it will be discussed later on, the effect of decreasing $p$ is to increase $B_\phi$ with respect to the other components, and consequently to increase the shear.

As it is apparent from equation (7), the limiting case $p \to 0$ results in a purely radial field whose field lines are directed either outwards or inwards (whence the name of split monopole). The directions of the field lines divide the sphere (i.e. the star) into several zones, and we can imagine field lines of opposite directions connecting at radial infinity (W95). Split monopole fields obtained for different multipolar orders differ from one another in the number of zones into which the sphere is split.
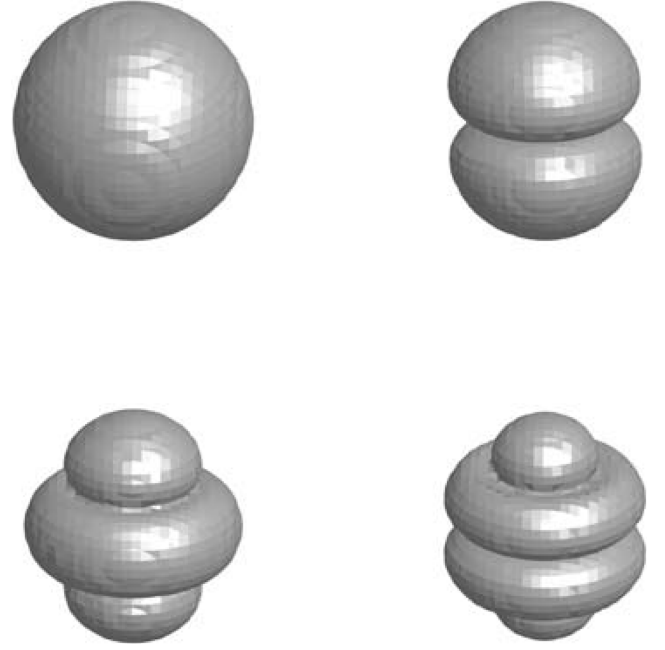
**Figure 1.** Zonal harmonics are used to visualize multipolar field topologies. From top left to bottom right: multipoles with order from one to four. The positions of the degenerate poles are evident.

### 2.1 Boundary conditions

In order to solve equation (8), we need to provide a suitable set of boundary conditions. For a dipolar field, there are just two poles and the star is divided into two hemispheres, i.e. the portions of the surface $0 \leq \theta \leq \pi/2$, $\pi/2 \leq \theta \leq \pi$, respectively, and $0 \leq \phi \leq 2\pi$. Higher order multipoles have in addition degenerate poles, which are loci of constant colatitude, and correspond to circles on the surface (see Fig. 1). For the quadrupole, for example, there are two poles on the magnetic axis and the equator is a degenerate pole. In the case of a generic multipolar field, the magnetic hemispheres of the dipole are replaced by a number of regions, each limited by two consecutive values of the colatitude, $\theta_i$, $\theta_{i+1}$, for which the field is purely radial (the pole) and has vanishing radial component (the magnetic 'equator'), i.e. $B_\theta(\theta_i) = 0$ and $B_{\mathrm{r}}(\theta_{i+1}) = 0$. We refer to these zones as to regions of unipolar $B_{\mathrm{r}}$.

Because of the north–south symmetry of unsheared multipolar fields, which is assumed to hold also for their twisted counterparts, the integration domain is restricted to $0 \leq \mu \leq 1$. In analogy with the 'composite magnetic fields' of Low & Lou (1990), integration is performed piecewise, going from one pole to the next one. In each interval, the boundary conditions for equation (8) are determined by the requirements that (i) $\boldsymbol{B}$ is purely radial at each pole and (ii) the intensity is not modified by the shear. The latter condition can be enforced either by assigning the field strength at one pole or the magnetic flux out of each region of unipolar $B_{\mathrm{r}}$; in both cases, the value must not change with the shear. For multipoles of odd order (dipole, octupole, ...), the first subdomain starts at the geometrical equator, $\mu = 0$, which is not a pole. In these cases, the boundary condition at $\mu = 0$ reflects the north-south symmetry of the field and translates into $f'(0) = 0$ (TLK).

The magnetic field in the entire interval ($0 \leq \mu \leq 1$) is then obtained by assembling the solutions computed in the various subdomains with the same value of $p$, to ensure that the radial dependence of $\boldsymbol{B}$ is the same at all colatitudes. Since the GSS equation is a

second order ODE, imposing three boundary conditions implies that the parameter $C$ is an eigenvalue of the problem and depends on the radial index $p$, $C = C(p)$. Each multipolar potential term satisfies the GSS equation with $C = 0$ and is associated to an integer radial index $p_0$; it is $p_0 = 1$ for the dipole, $p_0 = 2$ for the quadrupole and so on. In this particular case, the equation is linear and admits analytical solutions of the form (W95)

$$f_{p_0}(\mu) \propto \sqrt{1 - \mu^2} P^1_{p_0}(\mu), \tag{10}$$

where $P^1_p(\mu)$ is the associated Legendre function of the first kind (Abramowitz & Stegun 1972).

Having established a set of boundary conditions, the GSS equation can be solved for different values of $p$, building a sequence of models characterized by a varying shear. As shown by Low & Lou (1990), such a sequence shares the same topology, i.e. the same number and position of poles. The only permitted values of the radial index are $p \leq p_0$.

## 2.2 Dipolar fields

The generating function of a pure dipole is

$$f_{p_0=1} = 1 - \mu^2, \tag{11}$$

thus from equation (7) it follows that the condition at the pole $\mu = 1$ is $f(1) = 0$, to which the symmetry condition $f'(0) = 0$ must be added. The third condition is set either specifying the field strength at one pole, $f'(1) = 1$ (as in TLK), or requiring a constant flux, $f(0) = 1$ (W95). The sequence of sheared dipoles has radial index $0 \leq p \leq 1$.

Sheared dipole fields have been discussed by W95 and TLK. These investigations, however, used a different boundary condition (see above) and we verified that the numerical solution of equation (8) produces quite different results for $f(\mu; p)$ and even more diverse eigenvalues $C(p)$ in the two cases (see Fig. 2). Still, one expects the magnetic field to be the same in both cases, since the two boundary conditions are physically equivalent. Actually, a direct comparison of the numerical solutions shows that $f_{\mathrm{TLK}}/f_{\mathrm{W95}} \simeq f'_{\mathrm{TLK}}/f'_{\mathrm{W95}} \simeq$ constant for each $p$. Denoting by $\lambda(p)$
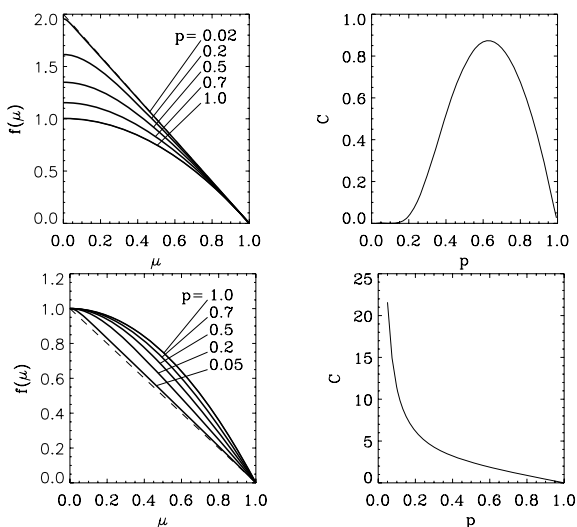


**Figure 2.** Upper panels: the function $f(\mu)$ and the eigenvalue $C$ for different values of $p$ with the prescription of constant $B_{\mathrm{pole}}$ (the dashed line in the left-hand panel is the analytical solution for $p \to 0$). Lower panels: same, but for constant flux.

**Table 1.** The eigenvalues $C(p)$ for the two different sets of boundary conditions and the ratio $\lambda = f_{\mathrm{TLK}}/f_{\mathrm{W95}}$ for $0 < p < 1$.

| $p$ | $C_{\mathrm{TLK}}$ | $C_{\mathrm{W95}}$ | $\lambda$ |
|------|------|------|------|
| 0.97 | 0.13 | 0.11 | 1.02 |
| 0.89 | 0.41 | 0.45 | 1.06 |
| 0.82 | 0.63 | 0.79 | 1.10 |
| 0.74 | 0.78 | 1.14 | 1.15 |
| 0.67 | 0.86 | 1.51 | 1.21 |
| 0.59 | 0.86 | 1.91 | 1.26 |
| 0.52 | 0.79 | 2.35 | 1.33 |
| 0.45 | 0.64 | 2.87 | 1.39 |
| 0.38 | 0.43 | 3.52 | 1.47 |
| 0.30 | 0.22 | 4.41 | 1.56 |
| 0.22 | 0.06 | 5.80 | 1.65 |
| 0.15 | $3.9 \times 10^{-3}$ | 8.52 | 1.75 |
| 0.07 | $4.3 \times 10^{-7}$ | 17.48 | 1.88 |
| 0.02 | $1.55 \times 10^{-25}$ | 89.78 | 1.97 |

this constant ratio, one can write the expression of the field in the two cases using equation (7):

$$\boldsymbol{B}_{\mathrm{W95}} \propto \left[ -f', \frac{p}{\sin\theta} f, \left( C_{\mathrm{W95}} \frac{p}{p+1} \right)^{1/2} \frac{f^{1+1/p}}{\sin\theta} \right]$$

$$\boldsymbol{B}_{\mathrm{TLK}} \propto \left[ -\lambda f', \lambda \frac{p}{\sin\theta} f, \left( C_{\mathrm{TLK}} \frac{p}{p+1} \right)^{1/2} \frac{(\lambda f)^{1+1/p}}{\sin\theta} \right], \tag{12}$$

where the radial dependence has been omitted. The two fields have the same topology if and only if

$$\lambda^{1+1/p} \sqrt{C_{\mathrm{TLK}}} = \lambda \sqrt{C_{\mathrm{W95}}}. \tag{13}$$

We checked that the previous condition is indeed satisfied by our numerical solutions with a relative accuracy of $\sim 2$ per cent for nearly all values of $p$.[1] The eingevalues and the ratio $\lambda$ for different values of $p$ are reported in Table 1.

The magnetic field, then, has the same topology in both cases, and the two solutions differ only for a multiplicative factor (which changes with $p$); i.e. it is $\boldsymbol{B}_{\mathrm{TLK}} = \lambda \boldsymbol{B}_{\mathrm{W95}}$, with $1 \leq \lambda \leq 2$. The great diversity in the eigenvalues, especially for $p \to 0$, is in fact balanced by the different behaviour of the function $f(\mu)$. While for constant $B_{\mathrm{pole}}$, it is $1 \leq \max f \leq 2$, in the case of constant flux $\max f = 1$ for any $p$. In the limit $p \to 0$, the proportionality of the two solutions for $f$ can be recovered analytically. In fact, it can be shown that in the split monopole limit, the generating functions are

$$f(\mu) = 1 - |\mu| \qquad \text{for constant flux}$$

and

$$f(\mu) = 2(1 - |\mu|) \quad \text{for constant } B_{\mathrm{pole}}$$

which give $\lambda(0) = 2$, in agreement with the numerical result (see again Table 1).

## 2.3 Higher order multipoles

Since equation (8) is the force–free condition for a generic axisymmetric field (as given by equation 2), axisymmetric globally-twisted multipoles can be found solving again equation (8), subject to the

---

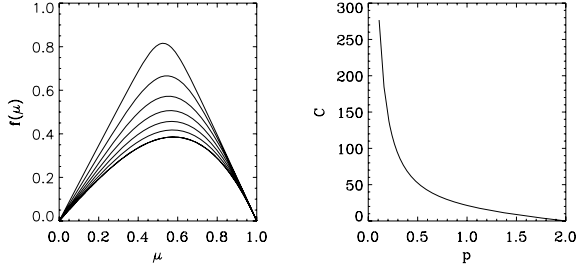[1] The error becomes larger for $p \sim p_0$ because $\lambda \sqrt{C_{\mathrm{W95}}} \to 0$.

**Figure 3.** Generating functions and eigenvalues for the quadrupolar fields. Different curves correspond to different values of $p$ from $p = 2$ (lower curve) to $p = 0.2$ (upper curve).
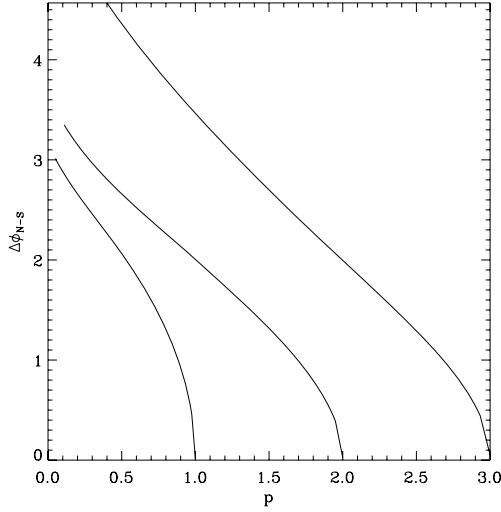


**Figure 4.** The shear angle $\Delta\phi_{\rm NS}$ as a function of $p$. The three curves correspond to dipolar quadrupolar and octupolar fields (from left to right).

boundary conditions discussed in Section 2.1. For an untwisted quadrupolar field, the generating function is

$$f_{p_0=2} = \mu(1 - \mu^2). \tag{14}$$

Within our integration domain $0 \leq \mu \leq 1$, the poles are located at $\mu = 0$ (degenerate) and $\mu = 1$. The boundary conditions are then

$$f(1) = 0, \tag{15}$$

$$f(0) = 0 \tag{16}$$

and

$$f'(1) = -2 \ {\rm or} f\left(\frac{1}{\sqrt{3}}\right) = \frac{2}{3\sqrt{3}}; \tag{17}$$

the latter two conditions enforce either constant field strength at the pole or constant flux, and, as discussed in the previous section, are equivalent. However, on a numerical ground, we found that for higher order multipoles the constant flux boundary condition is highly preferable and has been used in the calculations presented here. The field in $-1 \leq \mu \leq 0$ is obtained by symmetry. The quadrupolar angular functions $f(\mu)$ and eigenvalues $C(p)$ are shown in Fig. 3 for different values of $p$. The shear angle as a function of $p$ (equation 9) is shown in Fig. 4 (middle curve).

In the case of an untwisted octupole, instead, the generating function is

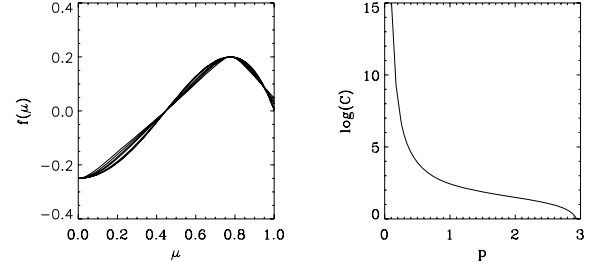$$f_{p_0=3} = \frac{1}{4}(1 - \mu^2)(5\mu^2 - 1) \tag{18}$$

**Figure 5.** Same as Fig. 3, but for octupolar fields; here $p$ is in the range [0.2, 3].

and the poles are located at $\mu = 1, 1/\sqrt{5}$ (again restricting to the range $0 \leq \mu \leq 1$). In order to compute the sheared field, equation (8) needs to be solved in two separate intervals, $0 \leq \mu \leq 1/\sqrt{5}$ and $1/\sqrt{5} \leq \mu \leq 1$. Taking into account that $\mu = 0$ is not a pole in the present case, the boundary conditions are

$$f(1/\sqrt{5}) = 0, \tag{19}$$

$$f'(0) = 0 \tag{20}$$

and

$$f'(1/\sqrt{5}) = \frac{2}{\sqrt{5}} \ {\rm or} \ f(0) = -\frac{1}{4} \tag{21}$$

in the range $0 \leq \mu \leq 1/\sqrt{5}$ and

$$f(1) = 0, \tag{22}$$

$$f(1/\sqrt{5}) = 0 \tag{23}$$

and

$$f'(1) = -2 \, {\rm or} f\left(\sqrt{\frac{3}{5}}\right) = \frac{1}{5} \tag{24}$$

in the range $1/\sqrt{5} \leq \mu \leq 1$. The numerical solutions are shown in Fig. 5 and the dependence of the shear angle on $p$ can be read from Fig. 4 (rightmost curve).

Despite the fact that numerical solution of equation (8) poses no problems, having analytical expressions for the twisted field components may prove handy in some applications. In Appendix A, we derive approximated analytical expressions for the generating function $f(\mu)$ for dipolar and quadrupolar configurations valid for small shear ($p_0 - p \ll 1$), compare them with the exact numerical solutions and discuss their ranges of validity.

## 3 SPECTRA AND LIGHTCURVES

In this section, we use the numerical code described in NTZ to explore the effects of different sheared multipolar fields on the emergent spectra and lightcurves of magnetars. Although the external field of a magnetar is unlikely to comprise a single higher order multipole, investigating spectral formation when the field is one (twisted) multipole offers the opportunity to explore the effects of magnetospheric currents localized on spatial scales smaller than that implied by the (twisted) dipole. An example is that of a sheared, localized component which appears as a consequence of some form of activity and adds up to a global,(quasi)potential dipolar field. The currents responsible for the resonant scatterings are provided only by the sheared field. The case, in which the localized component is modelled in terms of the polar 'lobe(s)' of an octupole, is
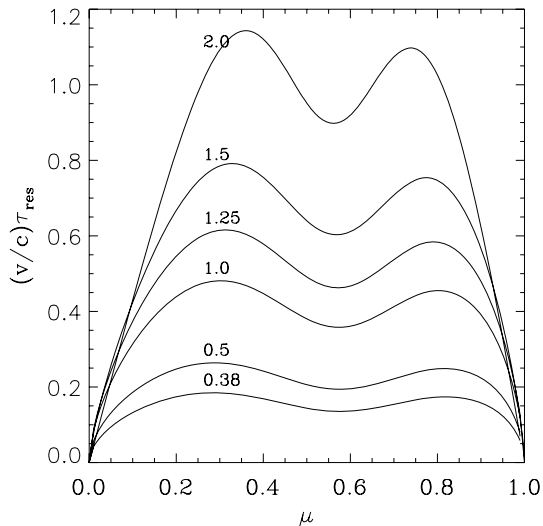
**Figure 6.** Optical depth to resonant cyclotron scattering at the resonant radius as a function of the colatitude for quadrupolar configurations; each curve is labelled by the value of the shear angle $\Delta\phi_{NS}$.

discussed in Section 3.3. We base our model on the scenario envisaged by TLK (see also Lyutikov & Gavriil 2006; Fernandez & Thompson 2007; NTZ, for more detailed calculations), according to which thermal photons originating at the star surface undergo repeated scatterings with the charge carriers (electrons, ions and possibly pairs; see also Beloborodov & Thompson 2007) flowing along the field lines. These investigations were based on non-relativistic computations, and therefore necessarily restricted to the low-energy ($\lesssim 10\,\mathrm{keV}$) emission. Furthermore, they were based on the dipolar, globally-twisted magnetosphere of TLK.[2]

### 3.1 Globally twisted multipoles

In order to gain some insight on the properties in the emitted spectra when the magnetosphere is threaded by twisted, higher order multipoles, we plot in Figs 6 and 7 the optical depth $\tau_{\mathrm{res}}$ to resonant scattering corresponding to quadrupolar and octupolar fields. This is given by

$$\left(\frac{v}{c}\right)\tau_{\mathrm{res}} \sim \frac{\pi}{4}\left(1+\cos^2\theta_{kB}\right)\left[\frac{C(1+p)}{p}\right]^{1/2}\frac{f^{1/p}}{2+p}, \qquad (25)$$

where $v$ is the charge velocity and $\theta_{kB}$ is the angle between the primary photon (assumed to move radially) and the magnetic field at the scattering radius (TLK). Since $v \sim c$, $(v/c)\tau_{\mathrm{res}} \sim \tau_{\mathrm{res}}$ and we make no further distinction between these two quantities. By comparing these curves to those in Fig. 8, we can clearly see that the optical depth for higher order multipoles is sensibly different from that of a dipolar configuration, implying that the overall spectral properties, and in particular those of the pulse phase emission, may be significantly affected. We remark that the typical radius at which resonant scattering occurs is different for the different multipoles. Assuming that the surface strength is comparable, scattering in higher order multipolar fields takes place closer to the star with respect to the dipole because the field decays faster with radius.

[2] The simplified, analytical model of Lyutikov & Gavriil (2006) did not assume a precise topology for the magnetic field.
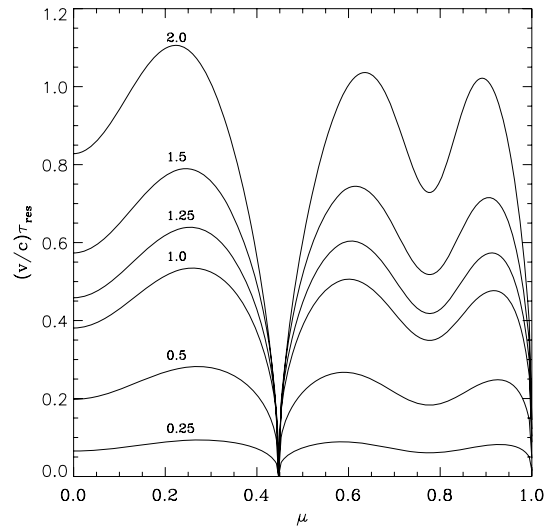


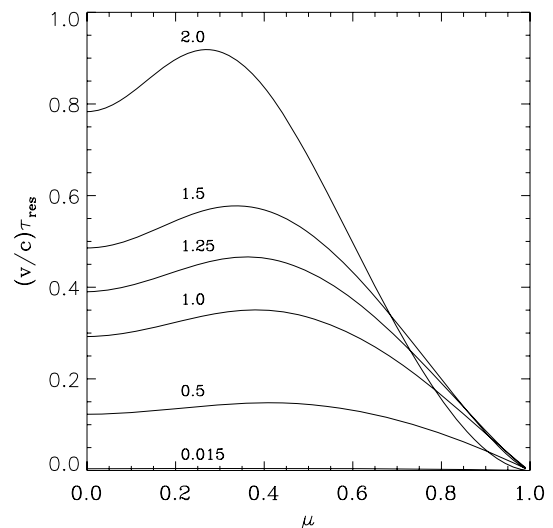**Figure 7.** Same as in Fig. 6, but for an octupolar field.



**Figure 8.** Same as in Fig. 6, but for a dipolar field.

To further investigate this, we calculated a number of synthetic spectra and lightcurves by using the non-relativistic Monte Carlo code by NTZ. A comparison among spectra produced by a globally twisted dipolar, quadrupolar and octupolar magnetosphere is shown in Fig. 9. Spectra have been computed for the same values of model parameters (blackbody temperature $kT_\gamma = 0.5\,\mathrm{keV}$, temperature and bulk velocity of the magnetospheric electrons $T_{\mathrm{el}} = 30\,\mathrm{keV}$, $\beta_{\mathrm{bulk}} = 0.5$, polar magnetic field strength $B_{\mathrm{pole}} = 10^{14}\,\mathrm{G}$) and for the same shear angle ($\Delta\phi_{NS} = 1.2\,\mathrm{rad}$, which corresponds to $p = 0.8$, 1.6, 2.5 for the dipole, the quadrupole and the octupole, respectively).[3] Spectra have been computed by collecting photons over the entire observer's sky (i.e. by angle-averaging over all viewing directions). The most prominent feature in Fig. 9 is the higher comptonization degree induced by the quadrupolar (and dipolar) field with respect

[3] Although these values of the model parameters can be regarded as typical (see NTZ), the present choice has only illustrative purposes. Other combinations of the parameters are equally possible and, provided that electrons remain mildly relativistic, will give similar results.
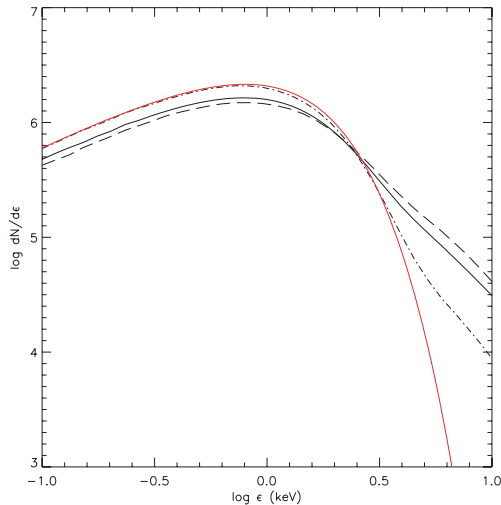
**Figure 9.** Monte Carlo spectra for globally twisted dipolar (solid line), quadrupolar (dashed line), octupolar (dash–dotted line) force free magnetospheres; the shear angle is the same in all three cases ($\Delta\phi_{NS} = 1.2$ rad). The solid red line is the seed blackbody spectrum. The total number of photons is $\sim 4 \times 10^6$ in all the simulations.



**Figure 10.** Spectra obtained with the Monte Carlo code for a locally twisted ($\Delta\phi_{NS} = 1.5$ rad, $p = 2.3$) octupolar force–free magnetosphere. The shear is equally distributed on both polar lobes, while in the equatorial zone the magnetosphere is potential. Different curves correspond to different viewing angles (blue $\Theta_S = 0°$, red $\Theta_S = 60°$, green $\Theta_S = 104.5°$, black $\Theta_S = 180°$); the dashed line is the seed blackbody spectrum.

to the octupolar one. This can be understood in terms of different spatial distribution of the scattering particles (see Figs 6–8) and of the different efficiency of scatterings, the latter depending on the (average) angle between the photon direction and that of the flowing currents. Upscattering is more efficient in regions where the currents move towards the star, i.e. close to the magnetic south pole(s), because collisions tend to occur more head-on (see also NTZ). For a dipolar field, the more favourable situation (i.e. large optical depth and currents flowing towards the star) arises for $\mu \sim -0.3$ (compare with the spectra at different viewing angles in fig. 1 of NTZ; the one at $\Theta_S = 116°$ is the more comptonized). For the quadrupole returning currents are localized around $\mu \sim 0$ (the geographical equator which is a degenerate south pole) and there are two regions with large optical depth in $0 \leq \mu \leq 1$ (see fig. 6). The one at $\mu \sim 0.3$ is closer to the south pole ($\mu = 0$) than in the case of the dipole, for which it occurs at $\mu \sim -0.3$ while the south pole is at $\mu = -1$. The reason for which octupolar twisted fields produce less efficient upscattering is that, despite there are two maxima of the optical depth located quite close to the south pole (at $\mu \sim 0.2, 0.6$, the south pole is at $\mu = 1/\sqrt{5} \sim 0.45$), the relatively large curvature of the field lines makes the angular extent of the region containing the currents narrow. As a consequence most photons scatter with electrons moving at large angles and this results in steeper spectra.

### 3.2 A simple localized twist model

There is now observational evidence that, at least in some cases, the magnetospheric twist in both SGRs and AXPs could be localized in restricted regions of the magnetosphere. For instance, Woods et al. (2007) found a certain degree of hysteresis in the long-term evolution of SGR 1806−20 prior to the emission of the GF in 2004 December, with a non-trivial correlation between spectral and timing properties that may be interpreted if only a small bundle of magnetic field lines is affected by the shear. A further case is provided by the spectral evolution of the transient AXP XTE J1810−197 (Bernardini et al. 2009; Perna & Gotthelf 2008) which seems to re-
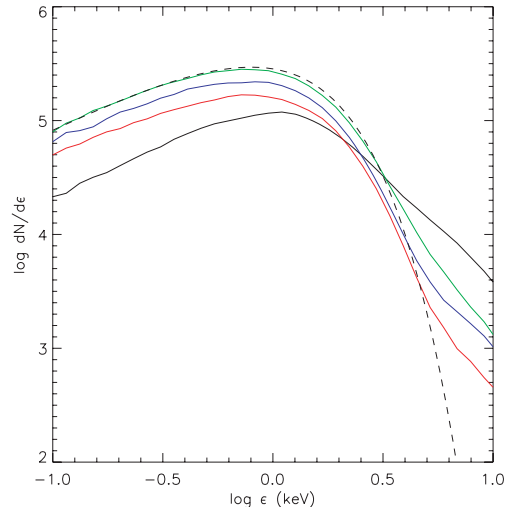
quire a twist concentrated towards the magnetic axis, giving rise to a polar hot region, possibly with a meridional temperature gradient.

Motivated by this, we investigated the possibility to model a localized twist, by constructing a solution in which the shear changes with the magnetic colatitude of the field line foot point. Although the configurations presented in the previous sections are globally twisted, the octupolar solution, which requires piecewise integration in two domains (see Section 2.3), can be used to construct a field with a non-vanishing twist at low-magnetic colatitudes. This is done by superimposing a sheared octupole for $0 \leq \mu \leq 1/\sqrt{5}$ to a potential one in $1/\sqrt{5} \leq \mu \leq 1$ and is equivalent to solve equation (8) in the entire domain with $p(\mu) = p* H(\mu - 1/\sqrt{5})$, where $H$ is the Heaviside step function and $p*$ a given constant. We note that, although not physically self-consistent, such a field is force–free (see the discussion in Section 4).

The Monte Carlo spectra for different viewing angles are shown in Fig. 10 in the case in which the field has equatorial symmetry, i.e. the shear $\Delta\phi_{NS} = 1.5$ rad ($p = 2.3$) is applied on both polar lobes while the equatorial zone is permeated by a potential octupole. The spectra for the more interesting case in which the same shear is confined only around one pole are plotted in Fig. 11.

### 3.3 Timing and spectral properties of magnetars high-energy emission

Spectral models which account for different magnetospheric configurations hold the potential to reproduce not only the gross features of the observed spectra but also the subtler properties which are revealed by the combination of very high-quality spectral and timing data. While a complete application is beyond the scope of this paper, here we consider our results in the context of the spectacular phase dependence which has been recently discovered in the hard X-ray tails of the two AXPs 1RXS J1708−4009 and 4U 0142+61 (Den Hartog et al. 2008a,b). These deep *INTEGRAL* observations have shown that, in both of these sources, there are several different pulse components (at least three) with genuinely different spectra.
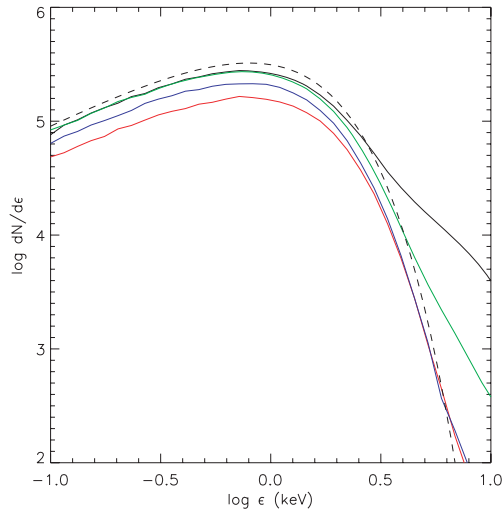
**Figure 11.** Same as in Fig. 10, but for the shear localized only at upper north pole.

The hard X-ray spectrum gradually changes with phase from a soft to a hard power law, the latter being significantly detected over a phase interval covering ~1/3, or more, of the period.

In order to see how these features can, at least qualitatively, be explained by our models, let us consider the locally twisted configurations discussed in Section 3.2 which, among those presented so far, provide the most significant variations of the magnetic topology with the colatitude. Let us introduce two angles, $\chi$ and $\xi$, which give, respectively, the inclination of the line of sight (LOS) and of the magnetic axis with respect to the star spin axis. This allows us to take into account for the star rotation and hence derive pulse profiles and phase-resolved spectra. Because of the lack of north-south symmetry, it is $0 \leq \chi \leq \pi$, while $\xi$ spans the interval $[0, \pi/2]$ (see NTZ for further details). For each viewing geometry, and for different values of the shear, we can now compute the optical depth (equation 25) as a function the rotational phase $\gamma$ ($0 \leq \gamma \leq 2\pi$). A few examples are shown in Fig. 12 for the case in which the twist is localized on two polar caps.

In connection with the spectral evolution with phase observed in 1RXS J1708−4009 and 4U 0142+61, the more favourable cases are those in which it is $(v/c)\tau_{res} > 1$ for roughly one third of the period. This is because resonant scattering over a population of (relativistic) electrons is then expected to be most efficient in producing a hard tail over the right phase interval, while the decrease of the depth at other phases results in a softening of the spectrum. A complete exploration of the parameter space aimed at searching for all configurations for which the previous condition is met is beyond the purposes of this paper. Just for illustrative purpose, let us consider one of those, i.e. an octupolar field with shear $\Delta\phi_{N-S} = 1.5$. By assuming this value and taking $\xi = 32°$ $\chi = 140°$, we then computed phase resolved spectra and energy-dependent lightcurves by using our Monte Carlo code. Since we are dealing with photon energies $\approx 100$ keV, at which electron recoil and relativistic effects may become important, we performed the runs using a relativistic version of the code (Nobili et al. 2008b; Nobili, Turolla & Zane, in preparation). Results are reported in Figs 13 and 15. Again in the spirit of probing the potentialities of our model, rather than presenting a detailed fit, the parameter values in the Monte Carlo runs are the same as those adopted in Section 3.2, $B_{pole} = 10^{14}$ G, $\beta_{bulk} = 0.5$, $T_{el} = 30$ keV and $T_\gamma = 0.5$ keV. We remark again
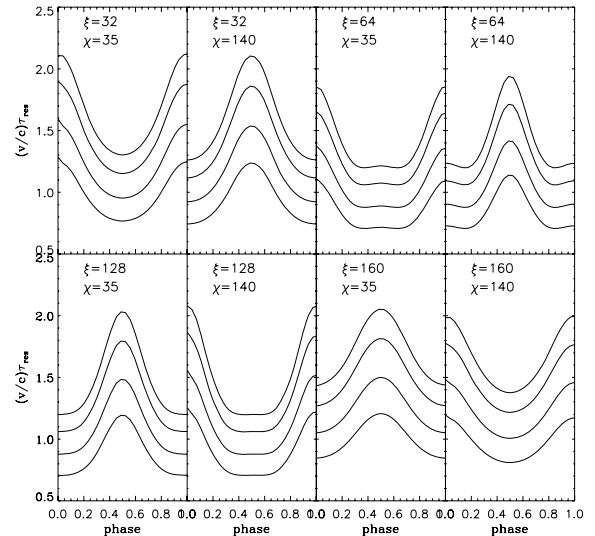


**Figure 12.** The depth $(v/c)\tau_{res}$ versus rotational phase for an octupolar field with twist located on the two polar caps. Each panel refer to different values of the geometrical angles $\chi$ and $\xi$ (see text for details). The curves in each panel are for $\Delta\phi_{N-S} = 1.22, 1.50, 1.78, 1.96$ from bottom to top.

that these values are not preferential, and that the results presented below do not critically depend on the model parameters.

As it can be seen from Fig. 13, for a magnetic configuration with the shear concentrated in a single lobe, resonant comptonization gives rise to a hard tail which is quite pronounced at the peak of the pulse while it is depressed by almost an order of magnitude at pulse phases close to the minimum of the hard X-ray lightcurve. This is similar to what has been observed in AXP 1RXS J1708−4009 and AXP 4U0142+61 (Den Hartog et al. 2008a,b). This model also predicts a considerable variation of the pulsed fraction with energy, ranging from a few percent below 2 keV to a few tens of percent from 2 to 10 keV and up to 90 per cent in the harder part of the spectrum. The comparison between modelled and observed phase-resolved spectra is beyond the scope of the present investigation.

For comparison we show in Fig. 14 the same results computed by assuming a globally twisted dipolar magnetosphere, with the same shear and taking the same parameters for the viewing geometry and the Monte Carlo run. It is clear that the pulse resolved spectra and lightcurves obtained in this case are completely different and can not reproduce those observed from the two AXPs. In this case, the hard part of the spectrum show very little variation with the rotational phase and the lightcurve dependence on the energy is opposite to that shown in Fig. 13, with a larger pulsed fraction expected in the soft band. Spectra and lightcurves obtained with a local twist applied at both polar regions produce results which, again, are not in agreement with observations (see Fig. 15).

## 4 DISCUSSION AND CONCLUSIONS

As first discussed by TLK, the external magnetic field of a magnetar likely possesses comparable poloidal and toroidal components. Twisted magnetospheres around ultramagnetized neutron stars have been shown to play a crucial role in shaping the emergent spectrum of SGRs/AXPs quiescent emission through efficient resonant scattering of thermal photons onto the charge carriers flowing along
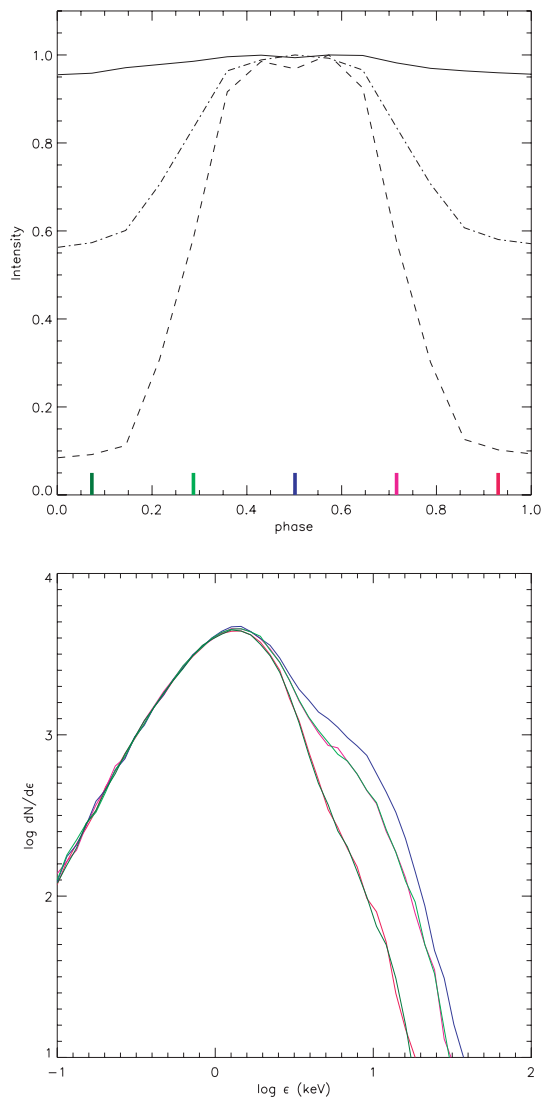
**Figure 13.** Synthetic lightcurves (upper panel) and phase-resolved spectra (lower panel) for a twisted magnetosphere with shear applied only to one polar lobe of an octupolar field (see text for details). In the upper panel, the solid, dash–dotted and dashed lines refer to the pulse profiles in the 0.5–2, 2–10 and 10–100 keV bands, respectively. In the lower panel, curves with different colours give the spectra at various phases; the colour code can be read at the bottom of the upper panel.

the field lines (Lyutikov & Gavriil 2006; Fernandez & Thompson 2007; NTZ).

In this paper, we tackled the problem of constructing sheared magnetic equilibria more general than a dipole. We have shown how sheared multipolar fields of arbitrary order can be computed by generalizing previous results by W95 and TLK. In order to assess the effects of different external field topologies on the emitted spectrum and pulse profiles, we ran a number of Monte Carlo simulations, using the code of NTZ, and compared the results to those of a sheared dipolar field. Not surprisingly, the overall spectral shape does not change in going from a dipole to higher order multipoles and can be always described in terms of a 'blackbody plus power law'. There are, however, quite substantial differences among the multipoles in the spectra viewed at different angles. These are mainly due to the different particle distribution in the magnetosphere which is directly related to the assumed field topology.
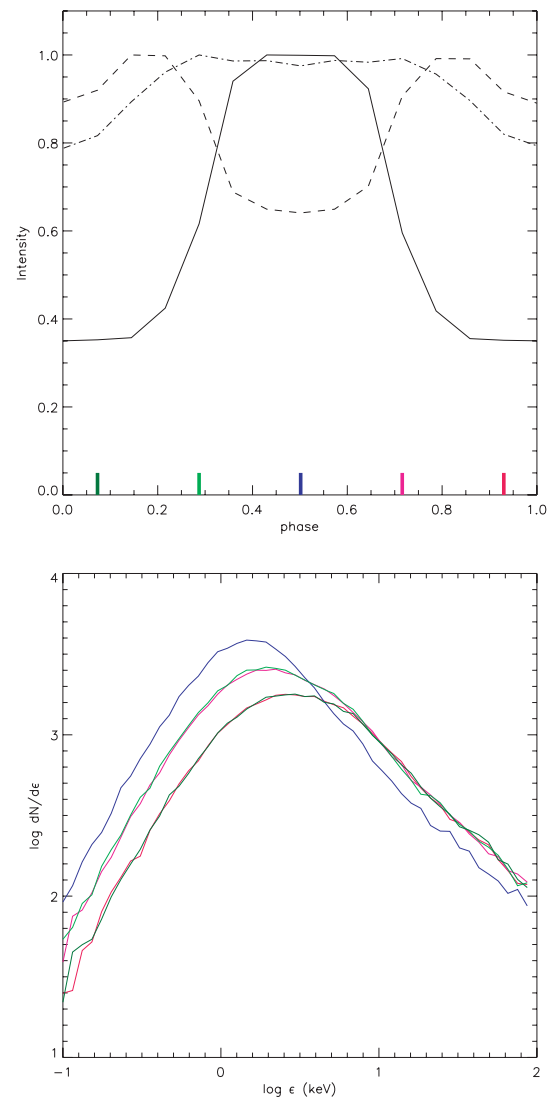
**Figure 14.** Same as Fig. 13 for a globally twisted dipolar field.

The case of an octupolar field has a special interest because it can be used to mimic a twist localized in a region close to the magnetic pole(s), and hence to investigate the properties of spectra produced in locally twisted magnetospheres. We have computed model spectra and lightcurves for the cases in which the twist is confined to one or both polar regions (each region has semi-aperture $\theta \sim 60°$), by assuming that only the polar lobes have a non-vanishing shear while the equatorial belt is potential. Quite interestingly, a twist confined to a single lobe is the only configuration, among those we have explored, that is able to reproduce the main features of the high-energy ($\sim$10–200 keV) emission observed with *INTEGRAL* from the AXPs 1RXS J1708−4009 and 4U 0142+61, in particular the large variation in the pulsed fraction at different energy bands (Den Hartog et al. 2008a,b).

All magnetic equilibria we discussed in this paper are globally twisted, axially symmetric multipolar fields. Of course, these configurations are far from being general and, even restricting to axial symmetry, represent only a subset of the solutions of the force–free equation. The magnetic field of a magnetar is likely to be quite complex. Modelling it in terms of single multipolar components offers a way of gaining insight on the general properties of
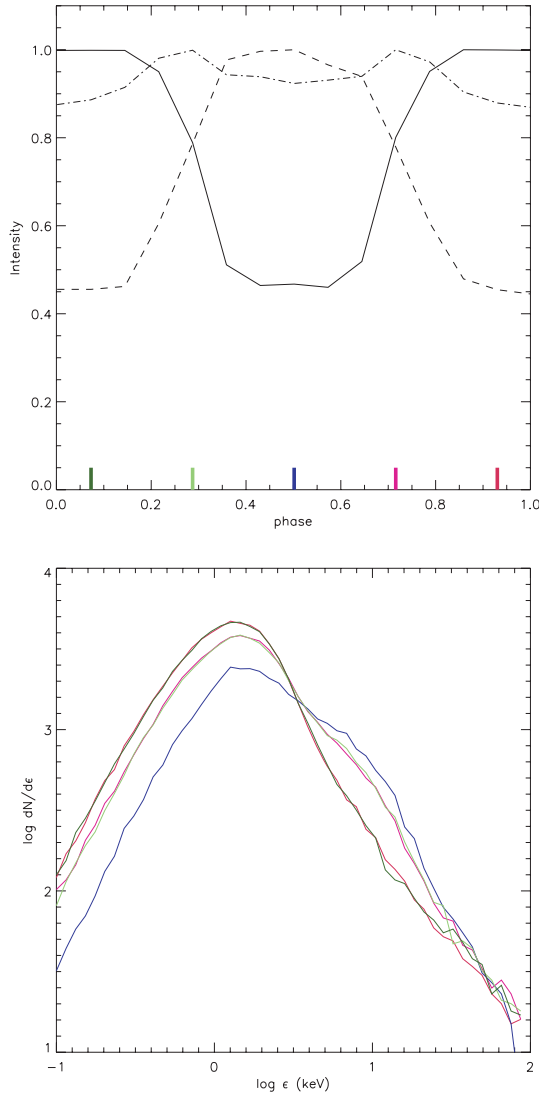
**Figure 15.** Same as Fig. 13 for the case in which the shear is applied to both polar regions.

the magnetosphere but is far from providing a realistic picture of these sources. A major obstacle in obtaining more complete models for the sheared field is non-linearity of the force–free equation. Given two force–free fields, $\boldsymbol{B}_1$ and $\boldsymbol{B}_2$, the linear combination $a\,\boldsymbol{B}_1 + b\boldsymbol{B}_2$ (with $a$ and $b$ two constants) is itself force–free only if $(\nabla \times \boldsymbol{B}_1) \times \boldsymbol{B}_2 + (\nabla \times \boldsymbol{B}_2) \times \boldsymbol{B}_1 = 0$. This implies that a generic sheared field cannot be expressed as an expansion of sheared multipoles, or, conversely, that the superposition of twisted multipoles is not a force–free field. An obvious case in which the previous condition is satisfied is that of potential fields. Since sheared fields depart smoothly from potential multipoles for $p \sim p_0$, for small enough twists a linear combination of force–free twisted multipoles (all with the same twist angle) may provide an approximate force–free field.

Despite many efforts have been devoted to develop techniques for solving the force–free equation, $\nabla \times \boldsymbol{B} = \alpha(\boldsymbol{x})\boldsymbol{B}$, no general, affordable method has been presented so far. The case of $\alpha$ a constant has been discussed long ago by Chandraskhar & Kendall (1957) and more recently by Mastrano & Melatos (2008), in connection with magnetars. If $\alpha$ is a known function of position, Cuperman &

Ditkowski (1991) presented an analytical method for solving the force–free equation also in the non-axisymmetric case. However, this is of little use for the problem of constructing self-consistent force–free magnetospheres since prescribing $\alpha$ is tantamount to assign the currents which sustain the field, while for the case at hand the field and the supporting currents depend on each other. A completely general, analytical technique has been proposed by Uchida (1997a,b). This is based on a relativistic (tensor) description of the electromagnetic field and on the introduction of two scalar potentials which are the analogues of the classical Euler potentials. It has been shown to be workable in the axisymmetric case (a non-aligned rotator, Uchida 1998), and for the particular case of a non-rotating, aligned magnetosphere, it is possible to verify that equation (8) is recovered. Further work on this is in progress and will be reported in a subsequent paper (Pavan et al., in preparation).

## REFERENCES

Abramowitz M., Stegun I. A., 1972, Handbook of Mathematical Functions. Dover, New York
Alpar M. A., 2001, ApJ, 554, 1245
Baring M., Harding A., 2007, Ap&SS, 308, 109
Baring M., Harding A., 2008, in Yuan Y.-F., Li X.-D., Lai D., eds, AIP Conf. Proc. Vol. 968, Astrophysics of Compact Objects. Springer-Verlag, Berlin, p. 93
Beloborodov A., Thompson C., 2007, ApJ, 657, 967
Bernardini F. et al., 2009, A&A, in press (arXiv:0901.2241)
Camilo F., Reynolds J., Johnston S., Halpern J. P., Ransom S. M., van Straten W., 2007a, ApJ, 659, L37
Camilo F., Ransom S. M., Halpern J. P., Reynolds J., 2007b, ApJ, 666, L93
Chandrasekhar S., Kendall P. C., 1957, ApJ, 126, 457
Cuperman S., Ditkowski A., 1991, A&A, 241, 646
Den Hartog P. R., Kuiper L., Hermsen W., Kaspi V. M., Dib R., Knödlseder J., Gavriil F. P., 2008a, A&A, 489, 245
Den Hartog P. R., Kuiper L., Hermsen W., 2008b, A&A, 489, 263
Duncan R. C., Thompson C., 1992, ApJ, 392, L9
Ekşi K. J., Alpar M. A., 2003, ApJ, 599, 450
Ertan Ü., Alpar M. A., 2003, ApJ, 593, L93
Fernandez R., Thompson C., 2007, ApJ, 660, 615
Feroci M., Hurley K., Duncan R. C., Thompson C., 2001, ApJ, 549, 1021
Götz D., Mereghetti S., Tiengo A., Esposito P., 2006, A&A, 449, L31
Low B. C., Lou Y. Q., 1990, ApJ, 352, 343
Kuiper L., Hermsen W., Mendez M., 2004, ApJ, 613, 1173
Kuiper L., Hermsen W., den Hertog P. R., Collmar W., 2006, ApJ, 645, 566
Lyutikov M., Gavriil F. P., 2006, MNRAS, 368, 690
Mastrano A., Melatos A., 2008, MNRAS, 387, 1735
Mereghetti S., Goetz D., Mirabel I. F., Hurley K., 2005, A&A, 433, L9
Mereghetti S., 2008, A&AR, 15, 255
Nobili L., Turolla R., Zane S., 2008a, MNRAS, 386, 1527 (NTZ)
Nobili L., Turolla R., Zane S., 2008b, MNRAS, 389, 989
Perna R., Gotthelf E. V., 2008, ApJ, 681, 522
Rea N., Zane S., Turolla R., Lyutikov M., Götz D., 2008, ApJ, 686, 1245
Thompson C., Duncan R. C., 1993, ApJ, 408, 194
Thompson C., Duncan R. C., 1995, MNRAS, 275, 255
Thompson C., Duncan R. C., 2001, ApJ, 561, 980
Thompson C., Beloborodov A. M., 2005, ApJ, 634, 565
Thompson C., Lyutikov M., Kulkarni S. R., 2002, ApJ, 574, 332 (TLK)
Uchida T., 1997a, Phys. Rev. E, 56, 2181

Uchida T., 1997b, Phys. Rev. E, 56, 2198
Uchida T., 1998, MNRAS, 297, 315
Wolfson R., 1995, ApJ, 443, 810 (W95)
Woods P. M. et al., 2005, ApJ, 629, 985
Woods P. M., Thompson C., 2006, in Lewin W., van der Klis M., eds, Cambridge Astrophysics Ser. 39, Compact Stellar X-ray Sources. Cambridge Univ. Press, Cambridge
Woods P. M. et al., 2007, ApJ, 654, 470

## APPENDIX A:

We start by expressing both the generating function and the eigenvalue $C$ in terms of a series expansion around the corresponding known untwisted quantities (labelled again with the index 0):

$$C = C_0 + \left(\frac{dC}{dp}\right)_{p_0} \Delta p + \cdots$$

and

$$f(\mu) = f_0(\mu) + f_1(\mu)\Delta p + \cdots,$$

where $\Delta p \equiv p - p_0$. By substituting the previous expressions into equation (8), we obtain, to first order in $\Delta p$,

$$(1 - \mu^2)f_1''(\mu) + p_0(1 + p_0)f_1(\mu) + (1 + 2p_0)f_0 +$$
$$\left(\frac{dC}{dp}\right)_{p_0} f_0^{1+2/p_0} = 0. \tag{A1}$$

It can be easily seen that equation (A1) admits analytical solutions only for integer values of the exponent $2/p_0$, i.e. for dipoles and quadrupoles for which $2/p_0 = 2$ and 1, respectively. Since $f_0$ is itself a solution of the GSS equation, it satisfies the same boundary conditions we need to impose on $f$. This implies that the conditions on $f_1$ are, in the case of a dipolar field, $f_1(1) = f_1'(0) = 0$, supplemented by either $f_1'(1) = 0$ or $f_1(0) = 0$. The two solutions that obey the previous two sets of conditions are

$$f_1(\mu) = f_0 \frac{-17 + 22\mu^2 - 5\mu^4}{32}$$
$$\left(\frac{dC}{dp}\right)_{p_0} = -\frac{35}{8}$$

and

$$f_1(\mu) = f_0 \frac{22\mu^2 - 5\mu^4}{32}$$
$$\left(\frac{dC}{dp}\right)_{p_0} = -\frac{35}{8},$$

respectively, where $f_0(\mu) = 1 - \mu^2$. The complete expressions for the two generating functions are then

$$f_{\text{W95}} \sim f_0 \left(1 + \frac{5f_0 + 17}{32}\mu^2 \Delta p\right),$$

$$f_{\text{TLK}} \sim f_{\text{W95}} - \frac{17}{32}f_0 \Delta p;$$

since $\Delta p < 0$, it is $f_{\text{W95}} < f_{\text{TLK}}$ for any value of the parameter in accordance with numerical results. A comparison of the first order approximations with the exact numerical solutions is shown in Fig. A1. We find that the agreement between the two is satisfactory (relative error $\lesssim 8$ per cent) up to $\Delta\phi_{\text{NS}} = 0.2$ in the case of fixed
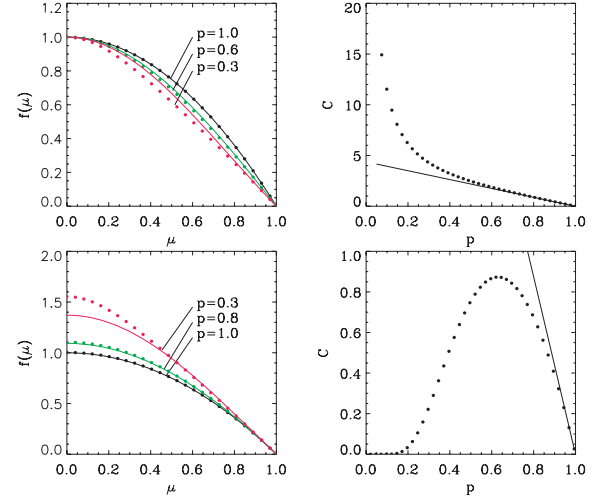


**Figure A1.** Dipolar angular functions $f(\mu)$ and eigenvalues $C(p)$ obtained with fixed flux (upper panels) and fixed $B_{\text{pole}}$ (lower panels). Solid lines represent the analytical first order approximation, while the dots are the numerical solutions of equation (8).
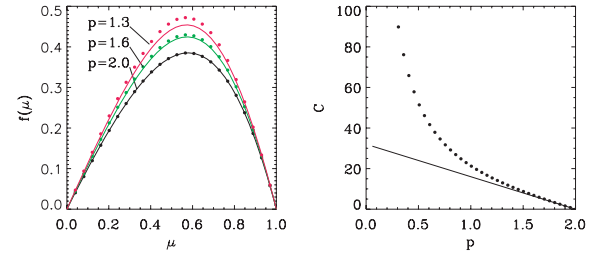


**Figure A2.** Same as in Fig. A1 for the quadrupolar field.

intensity and $\Delta\phi_{\text{NS}} = 0.4$ in the case of constant flux. The ratio $\lambda = f_{\text{TLK}}/f_{\text{W95}}$ introduced in Section 2.2 can be expanded as

$$\lambda(p) = 1 - \frac{17}{32}\Delta p.$$

By applying the same procedure, one can derive the analytic first order expansion for quadrupolar fields. For $f_1(1) = f_1(0) = f_1'(1) = 0$, the first two terms in the expansion of $f$ turn out to be

$$f_0(\mu) = \mu(1 - \mu^2),$$

$$f_1(\mu) = f_0 \left[\frac{3(1 - \mu) - 8\mu^2}{6(1 + \mu)} + \frac{2}{3}\mu^3 + \ln(1 + \mu) - \ln 2\right]$$

together with

$$\left(\frac{dC}{dp}\right)_{p_0} = -16.$$

The generating function $f$ and $C(p)$ are shown, together with the numerical solutions, in Fig. A2.

This paper has been typeset from a TeX/LaTeX file prepared by the author.